Three methods for characterizing thermo-optic noise in optical cavities

Elizabeth M. Gretarsson and Andri M. Gretarsson

Phys. Rev. D **98**, 122004 — Published 17 December 2018

DOI: 10.1103/PhysRevD.98.122004

Three methods for characterizing thermo-optic noise in optical cavities

Elizabeth M. Gretarsson*
College of Optical Sciences, University of Arizona, 1630E. University Blvd., Tucson, AZ 85721

Andri M. Gretarsson
Embry-Riddle Aeronautical University, 3700 Willow Creek Rd., Prescott, AZ 86301

Thermo-optic noise is likely to be the dominant noise source in next generation ultra-low noise optical cavities. We developed three measurement and analysis methods allowing us to estimate the level of coating thermo-optic noise in optical cavities, including interferometric gravitational wave detectors. We measured the shift in the broadband transmission spectra as a function of temperature for single-layer, high index coatings in order to find the thermo-optic coefficient, β_H, of a coating while assuming the thermal expansion coefficient, α_H. Our value for β_H could then be used to calculate the thermo-optic noise in any high-finesse optical cavity using coatings with the same high index layer material. We also measured the spectra as a function of temperature of a multi-layer, high-reflective coating where the material composition of the layers was similar to the coatings installed in Advanced LIGO. This method has the advantage of allowing us to calculate thermo-optic noise directly; α_H and β_H don't need to be known separately although we do need to know the value of the overall coating thermal expansion coefficient. Finally, we used lasers of different wavelengths to measure transmission changes on the band edges of a multi-layer high reflective coating. This gave measurements with high statistical precision but potentially lower systematic accuracy. To address systematic accuracy concerns, we used a constrained Monte-Carlo application of the theory of multilayer coating transmission.

I. INTRODUCTION

Optical phase fluctuations imparted upon a cavity beam by thermodynamic equilibrium fluctuations [1, 2] of mirrors limits the performance of some high sensitivity instruments. Equilibrium temperature fluctuations cause the optical pathlengths and thickness of high reflective coatings to fluctuate, leading to coating thermo-optic noise [3]. Thermo-optic noise is a coherent sum of the thermo-elastic noise [4–6] and thermo-refractive noise [7]. Coating thermo-optic noise is now a dominant noise source in some ultra-low noise optical reference cavities [8]. Similarly, the astronomical reach of the Advanced LIGO gravitational wave detector [9, 10] is limited in its most sensitive band by four noise sources, three of which are driven by thermodynamic equilibrium fluctuations. At it's projected sensitivity [11], the largest contributor to the Advanced LIGO noise budget in the high-sensitivity band (50-300 Hz) is coating Brownian noise (i.e. Brownian motion of the highly reflective surfaces of the primary interferometer mirrors) [12, 13]. The preparation of coatings with low Brownian noise is currently an active area of research [14–17]. Quantum noise [18] lies immediately below coating Brownian noise. At about one fourth of the quantum noise amplitude minimum, substrate brownian noise and coating thermo-optic noise appear.

One way to estimate the level of thermo-optic noise in an optical cavity is to apply the theory in [3]. This requires the thermal expansion coefficients α_H, α_L and the thermo-optic coefficients β_H, β_L of the high and low index coating materials, respectively. In some cases these coefficients are not known very accurately. In this paper we describe optical transmittance measurements of coatings for estimating coating thermo-optic noise. Since the optical thicknesses, L, of the coating layers have the largest effect on the coating transmittance, our measurements are sensitive to the quantity

$$\alpha + \beta/n = \frac{1}{L}\frac{dL}{dT} \tag{1}$$

where T is temperature and n is the refractive index of the coating layers. To obtain a specific value of β, n and α need to be obtained separately.

In Section II A, we describe measurements of the transmission spectrum of a single 5 μm, Ta_2O_5 coating layer as a function of temperature. These measurements give the combination $\alpha_H + \beta_H/n_H$ for the coating. They also give the value of n_H. To obtain a value for β_H, we used a literature value for α_H. (Here, we use the subscript "H" despite the fact that there is only a single layer because Ta_2O_5 is a common high index layer material in multilayer coatings.)

The properties of the thin layers within a multilayer coating may be different from the properties of a thicker single layer lying on the surface. The goal of the spectrum measurements described in Section II B was to measure $\alpha_H + \beta_H/n_H$ for the high index layers of a high-reflective quarter-wave stack. In a multilayer coating, the optical effects of α_H, α_L, β_H, and β_L are combined in a way that makes it difficult to separate the effects of optical thickness changes in the high versus low index layers.

*ejesse@optics.arizona.edu

This is compounded by the presence of unavoidable uncertainties in the as-deposited layer optical thicknesses. Nonetheless, since the low index layer material in our coatings was fused silica, which is quite well characterized in both bulk and thin film forms, literature values for α_L and β_L are likely to be accurate. If we assume the literature values for α_L and β_L, then our measurements give $\alpha_H + \beta_H/n_H$ as intended.

We also discovered that we could obtain an estimate for the thermo-optic noise in a cavity *directly* from our measurements without assuming any values for the individual parameters, α_H, α_L, β_H, and β_L. We just need to know the wavelength motion with temperature of the transmission minimum (center wavelength, λ_0) of the coating and the thermal expansion coefficient $\bar{\alpha}_c$ of the coating taken as a whole. The wavelength motion of the spectrum per unit temperature $\frac{d\lambda}{dT}$ is a function of wavelength

$$f(\lambda) \equiv \frac{d\lambda}{dT} \tag{2}$$

We measured $f(\lambda_0)$ but $\bar{\alpha}_c$ must be measured separately. A significant advantage of this method is that one only needs to measure two parameters rather than the four parameters required to apply [3] directly.

In Section II C, we describe measurements to monitor transmittance changes at laser wavelengths lying on the high-reflectivity band edges of a multilayer coating. We then use our measurements to find the motion of the of the center wavelength with temperature. This constitutes an independent measurement of $f(\lambda_0)$. These measurements however are more statistically precise, due to the large reflectivity changes observed and due to the high brightness of lasers as compared to broadband lamps. On the other hand, we had some concerns about systematic accuracy which we addressed by the use of a constrained Monte-Carlo technique.

In Section III, we discuss the possible influence of coating strain on the interpretation of our measurements. While coating strain is not expected to affect our estimates of thermo-optic noise, it may play a role in explaining the variation of coating β's in the literature.

In section Section IV, we make estimates of the thermo-optic noise. As mentioned above, we found a way of predicting the thermo-optic noise directly from the wavelength motion with temperature of the coating's center wavelength. The theoretical treatment explaining how that works is described in Section IV. In Section IV A, we give estimates of the thermo-optic noise contribution to a typical ultra-low noise reference cavity with an amorphous dielectric coating, based on our measurements. In Section IV B, we give estimates of the thermo-optic noise contribution to the Advanced LIGO noise budget.

Coating parameters found in the literature and relevant to this paper are gathered in Table I.

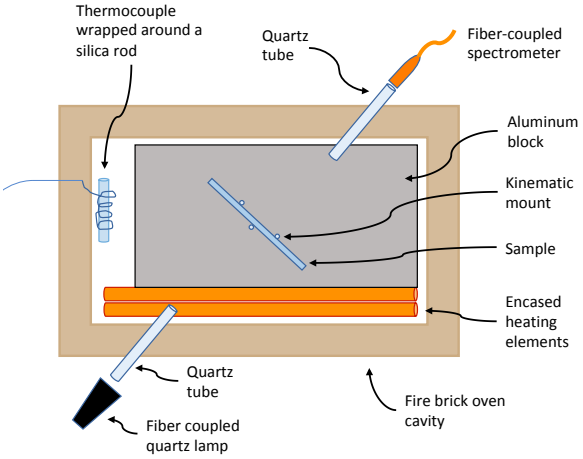

FIG. 1: Horizontal cross-section of the oven cavity, top view. This setup was used for measuring transmission spectra as a function of temperature. The setup was similar for the laser line transmittance measurements.

II. MEASUREMENTS

A. Transmission spectra of single layer coatings

We obtained transmission spectra as a function of sample temperature by heating a sample in an oven while shining light from a fiber coupled QTH (quartz tungsten halogen) lamp through the sample via small holes in the oven walls. Figure 1 shows the setup. The samples were polished silica disks of diameter 3" and thickness 3/32" with an ion beam deposited coating on one surface. We made measurements on two such samples. One had a 5 μm Ta_2O_5 single-layer coating. The other had a 500 nm ZrO_2-doped Ta_2O_5 coating; the molar fraction of ZrO_2 was 34%.

It was important to keep the sample at a uniform temperature and at the same temperature as the thermocouple. This was achieved by ensuring that all components within the oven were in thermal equilibrium with each other and with the oven walls. The oven walls were made with fire bricks, giving a 4" wall thickness. A large aluminum block (3"x5"x1.5") was placed under the sample holder to provide a uniform heat reservoir within the oven. The thermal time constant of the sample is about 5 minutes while that of the oven is over 1 hour. In such a setup, the components within the oven exchange heat much more quickly than the oven exchanges heat with the outside, ensuring that the components inside the oven cavity are at similar temperature. The uniformity of the temperature within the oven cavity was measured directly and found to vary by 5%, primarily vertically. Since the sample and thermocouple are at a similar height in the oven, their temperature should differ by less than five percent.

To start a measurement run, the oven was heated to

Symbol	Name	SI Unit	SiO_2	Ta_2O_5	15% TiO_2/ 85% Ta_2O_5
C	Heat cap. per unit vol.	$10^6\,J\,K^{-1}\,m^{-3}$	1.64 [19, 20]	2.51 [21, 22]	1.86 [23]
ρ	Mass per unit volume	$kg\,m^{-3}$	2200 [19, 20]	6850 [22]	5500 [17]
κ	Thermal conductivity	$W\,m^{-1}\,K^{-1}$	1.38 [19, 20]	33 [24]	28 [25]
n	Index of refraction	–	1.45 [19]	2.03 [24]	2.070 [26]
α	Thermal expansion coeff.	$10^{-6}K^{-1}$	0.51 [19, 20]	3.6 [27]	3.9 [28]
β	Thermo-optic coefficient	$10^{-6}K^{-1}$	8 [29]	–	–
E	Youngs Modulus	GPa	72 [19, 20]	140 [22]	162 [17]
ν	Poison ratio	–	0.17 [19, 20]	0.23 [24]	0.27 [17]

TABLE I: Values of various coating parameters obtained from the literature. For the materials that are mixtures, coefficient values for the individual materials were weighted by their molar fractions to calculate the coefficient for the mixture.

the maximum measurement temperature (around 300 °C) and kept there for an hour or more. The oven was then turned off and transmission spectra were recorded during the cool down period. To prevent systematics, we avoided the use of windows or fibers to couple light into or out of the oven. Instead, 5" long glass tubes with inner diameter 1/4" were placed diagonally through the oven walls. The air volume exchanged by the slight convection through these openings has very small heat capacity and cannot affect the sample temperature significantly. However, the thermocouple's heat capacity is small; to reduce any effect on the thermocouple, we wrapped it tightly around a 3/8"x3" fused silica rod.

It was also important to ensure that the sample remained stationary relative to the beam during measurement runs. This was acheived by constructing a "kinematic" mount for the sample out of fused quartz which has a very low thermal expansion coefficient. The mount had three legs and also three contact points to the sample.

The recorded spectra have numerous minima (maxima) occuring at wavelengths where the coating thickness corresponds to an odd (even) number of quarter wavelengths in the coating. The locations of these extrema provide a measurement of the coating's optical thickness. To find the change in the optical thickness as a function of temperature, we performed a parabolic fit to each extremum in spectra taken at different temperatures. See Fig. 2. The motion of the spectrum towards longer wavelengths with rising temperature is clear, indicating an increase in the coating's optical thickness with temperature, i.e. $f(\lambda) > 0$.

We monitored the motion of the extrema, obtaining the values $f(\lambda_j)$, where λ_j are the extrema locations, $j = 1, 2, \ldots$. In this section, $j = 1$ corresponds to the longest wavelength extremum in a given spectrum and j increases towards shorter wavelengths. The optical thickness of the coating at room temperature was found by fitting the wavelengths of the extrema in the spectrum data to the function

$$\lambda_j = \frac{4L}{N_1 + j - 1} \tag{3}$$

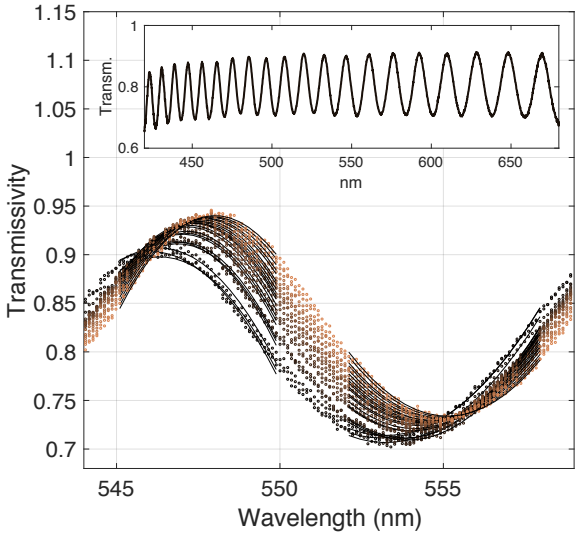

FIG. 2: The inset figure shows an example of the full transmission spectrum of a 5 μm thick, single layer, Ta_2O_5 coating on a fused silica substrate. The main part of the figure shows parabolic fits to two of the extrema at multiple oven temperatures. The extrema move towards longer wavelengths with increasing temperature.

The fit parameters are L and N_1. L is the optical thickness of the coating and N_1 is the number of quarter wavelengths in the coating at the longest wavelength extremum in the spectrum data (wavelength λ_1). Changes in the optical path correspond to changes in the extrema positions. The optical path change with temperature (1) at wavelength λ_j is

$$\alpha_H + \beta_H/n_H = \left(\frac{N_1 + j - 1}{4L}\right) f(\lambda_j) \tag{4}$$

The straight line fit to the coating optical thickness as a function of temperature for a particular run is shown in Fig. 3. The slope gives $\alpha_H + \beta_H/n_H$. We did observe a slight (but noisy) downwards trend in $\alpha_H + \beta_H/n_H$ towards higher wavelength [41]. It's unclear whether this is

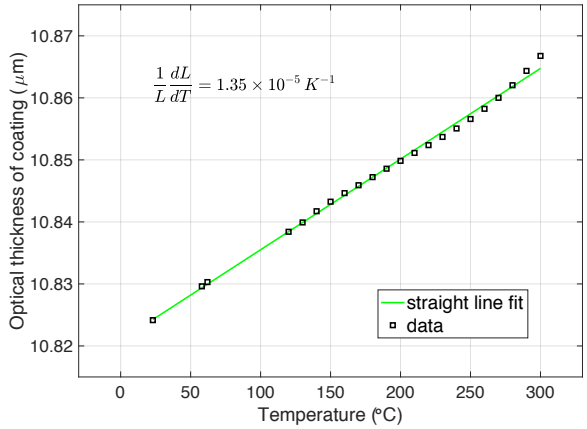

FIG. 3: Optical thickness versus temperature of the 5 μm Ta_2O_5 coating.

Single layer coating	$\alpha_H + \beta_H/n_H$ K^{-1}	n^*	$\beta^\dagger$ (K^{-1})
Ta_2O_5 L = 5 μm (10 measurements)	13.9 ± 1 $\times 10^{-6}$	2.17	22×10^{-6}
Ta_2O_5 (66%) doped with ZrO_2 (34%) L=500 nm (2 measurements)	18.6 ± 1 $\times 10^{-6}$	2.82	N/A

TABLE II: Single layer results. All coatings are on fused silica. The uncertainty in the individual values of n is a few percent, dominated by uncertainty in the thickness of the coatings. We estimate that the uncertainty in the individual measurements of $\alpha_H + \beta_H/n_H$ was about 10%, dominated by the fact that the estimates of the locations of the extrema depend slightly on the exact domain chosen for the parabolic fits. For the 5 μm Ta_2O_5 sample for which we have 10 measurements, this implies about 3% uncertainty in β.

* The index is reported at room temperature.
† Assumes $\alpha = 3.6 \times 10^{-6}$ K^{-1} for Ta_2O_5 coatings [6]. No value for β can be given for the Ta_2O_5/ZrO_2 coatings due to the lack of a measurement of α.

a physical or instrumental effect, so we averaged the optical thickness over the extrema in the wavelength range of the spectrometer (400 − 700 nm). Table II summarizes the results obtained for two different single layer coatings.

B. Transmission spectra of a multi-layer coating

We measured the temperature induced motion of the transmission extrema $f(\lambda_i)$ of a multilayer coating deposited on a polished fused silica substrate with diameter 3" and thickness 3/32". In this section, we count the extrema from the center wavelength of the coating, λ_0, so the index can take both positive and negative values ($i = \ldots\text{-}1, 0, 1, \ldots$). As before, we fit parabolas to the extrema of the transmission spectra at different temperatures. Fig. 4 shows the the shift of the extrema as a function of optical wavelength for a quarter wave stack with layer material compositions similar to the Advanced LIGO test mass coatings. We refer to this particular coated sample as "LMA5**". While, generally increasing with wavelength, the shift $f(\lambda_i)$ varies in a fairly complex manner, evincing the complexity of the underlying theory of multilayer coating transmission. We fit the extrema motion to that theory with β_H and α_H as fit parameters. α_L, β_L, and other coating parameters were taken from the literature (Table I). As expected, the Chi-squared distribution for the fit has a long valley along a line $\alpha_H + \beta_H/n_H$ = Constant, indicating that we've only measured the combination $\alpha_H + \beta_H/n_H$ with any accuracy and not α_H and β_H individually. The fit gives the result $\alpha_H + \beta_H/n_H = (28 \pm 8) \times 10^{-6}\,K^{-1}$. Extrapolating the model to the center wavelength gives the expected shift in the transmission spectrum at the center wavelength, $f(\lambda_0) = (-20 \pm 3)$ pm K^{-1}. From this value, in conjunction with the thermal expansion coefficient of the coating as a whole, $\bar{\alpha}_c$, we can calculate the thermo-optic noise in any cavity with similar coatings.

We feel that this approach has the greatest promise for characterizing thermo-optic noise in cavities as accurately and directly as possible. Unfortunately, the wavelength range of our spectrometers was not ideal. One should really measure the transmittance spectrum on both sides of the high reflectivity band. In our case, we are forced to extrapolate quite far into the infrared. Although, the nominal uncertainty in the final result is only about 15%, we don't know how seriously systematics affect the extrapolation. Therefore, in this section, we concentrate on the method and don't expect accurate results. Future measurements, applying this same method but using a spectrometer whose range covers both sides of the spectrum around the high-reflectivity band, should yield better estimates. Table III shows the current result.

C. Band edge transmittance

In this section we describe measurements of the transmittance versus temperature of the sample "LMA5**" at two laser wavelengths. The laser wavelengths λ_l, λ_r and corresponding angles of incidence Θ_l, Θ_r were chosen to lie on the left and right edges of the high reflectivity band, respectively. See Fig. 5.

The basic results of the measurements described in this section are estimates of the spectrum motion with tem-

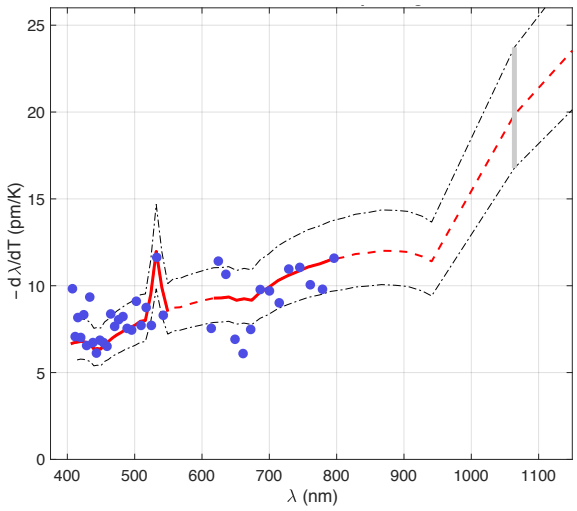

FIG. 4: Wavelength motion of the extrema with temperature for the LMA5** coating. Each data point represents a transmission minimum or maximum of the multilayer coating. The room temperature wavelengths of the extrema are shown on the x-axis. The extrema move towards longer wavelength with increasing temperature (or equivalently, the wavelength axis shifts toward the origin) so, the sign of $\frac{d\lambda}{dT}$ is negative. Typical motion is around -10 picometers per Kelvin. The fit is illustrated by the solid red line and gives $\alpha_H + \beta_H/n_H = (28 \pm 3) \times 10^{-6}$. The dashed red lines illustrate the model as extended the to the center frequency of the coating at 1064 nm. The dashed black lines correspond to the model with plus and minus one uncertainty in the fit parameters. At $\lambda_0 = 1064$ nm, this gives the center wavelength motion: $f(\lambda_0) = (\text{-}20 \pm 3)$ pm K^{-1}, indicated by the grey line in the upper right of the figure.

Multi-layer coating	$\alpha_H + \beta_H/n_H$ K^{-1}	$f(\lambda_0)$ pm K^{-1}
TiO_2-doped Ta_2O_5/SiO_2 15 $\lambda_0/4$ bi-layers $\lambda_0 = 1064$ nm, LMA5**	28 ± 8 $\times 10^{-6}$	-20 ± 3

TABLE III: Multilayer coating result (15 bi-layers). The high index layers are Ta_2O_5 doped with 15% (molar ratio) TiO_2.The low index layers are SiO_2. The layer materials in this coating are very similar to those used on the Advanced LIGO test masses. The result for $\frac{d\lambda}{dT}$ can be therefore be used to estimate the thermo-optic noise contribution directly.

perature at these two laser wavelengths and corresponding incident angles. Namely,

$$f(\lambda_l, \Theta_l) \equiv \left.\frac{d\lambda}{dT}\right|_{\lambda_l,\Theta_l} \quad \text{and}$$
$$f(\lambda_r, \Theta_r) \equiv \left.\frac{d\lambda}{dT}\right|_{\lambda_r,\Theta_r} .$$

As in Section II B, we then obtain an estimate for

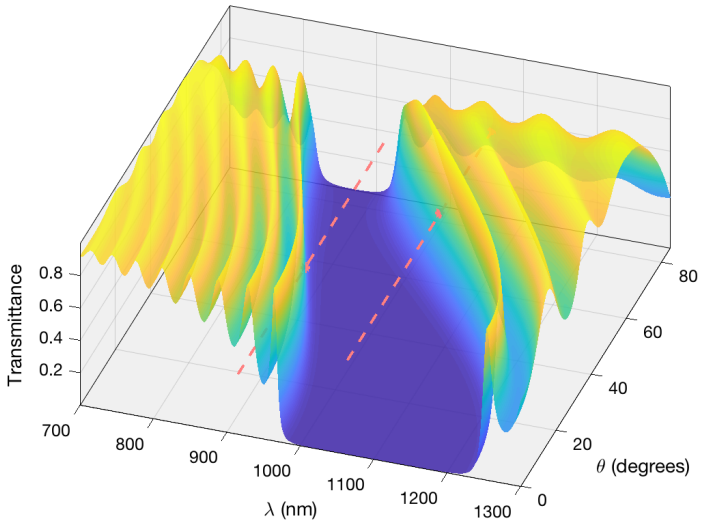

FIG. 5: Theoretical transmittance for the LMA5** sample for p-polarized light and nominal values of the coating parameters. The dashed lines indicate the interrogating laser wavelengths, $\lambda_l = 915$ nm and $\lambda_r = 1064$ nm.

the motion of the center wavelength with temperature, $f(\lambda_0, \Theta_0)$, at the design angle of incidence $\Theta_0 = 0$.

The setup was similar to that shown in Figure 1, except that the fiber coupled lamp was replaced with a 915 nm laser and the fiber-coupled spectrometer was replaced with a calibrated photodiode. Also, a second set of glass tubes was placed through the oven to accommodate a simultaneous measurement with a 1064 nm laser at a different angle of incidence.

We measured the rate of transmittance changes with temperature $\frac{d\,\text{Trans}}{dT}$ on each side of the band edge, (λ_l, Θ_l) and (λ_r, Θ_r) respectively. See Fig. 6.

On the band edge, transmittance changes with temperature are dominated by motion of the band edge to slightly longer or shorter wavelengths. The desired quantities $f(\lambda_l, \Theta_l)$ and $f(\lambda_r, \Theta_r)$ are well approximated by

$$f(\lambda_l, \Theta_l) = \frac{\left.\frac{\mathrm{d\,Trans}}{dT}\right|_{\lambda_l,\Theta_l}}{\left.\frac{\mathrm{d\,Trans}}{\mathrm{d}\lambda}\right|_{\lambda_l,\Theta_l}} \qquad (5)$$

and similarly for $f(\lambda_r, \Theta_r)$.

We used the standard theory of reflection for multilayer dielectric coatings to evaluate the band edge slopes $\frac{d\,\text{Trans}}{d\lambda}$ on each side of the band edge, at (λ_l, Θ_l) and (λ_r, Θ_r) respectively. We found that our initial estimates of the band-edge slopes were extremely sensitive to our choices for the coating layer thicknesses and the layer indices. The estimates were also very sensitive to the angle of incidence, so that variations in any of these parameters within their uncertainties led to unacceptably large variations in the band edge slope estimates. On the other hand, we measured the transmittance accurately and with good statistical precision. If we only allowed combinations of coating parameters and incidence angles

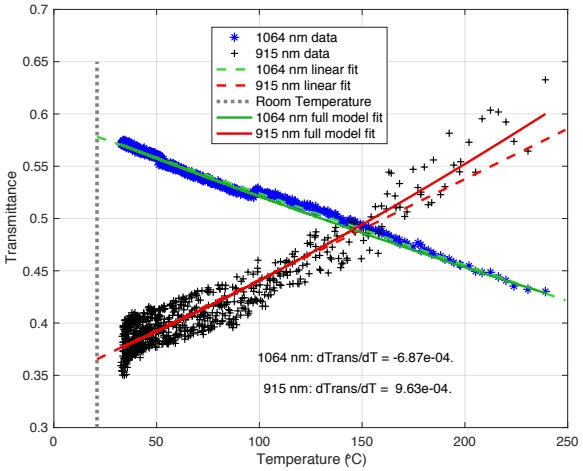

FIG. 6: The transmittance versus temperature for the LMA5** sample taken at wavelengths $\lambda_l = 915$ nm, $\lambda_r = 1064$ nm and correpsponding angles of incidence $\theta_l = (28.1 \pm 3.2)^\circ$, $\theta_r = (47.6 \pm 1.4)^\circ$. The response is largely linear but due to the large reflectivity changes seen, the full theory of multilayer reflection is needed to capture the high temperature behavior for the 915 nm measurement. The slopes $\frac{d\text{Trans}}{dT}$ are taken from the fits extrapolated to room temperature (where the fit lines meet the vertical dashed line).

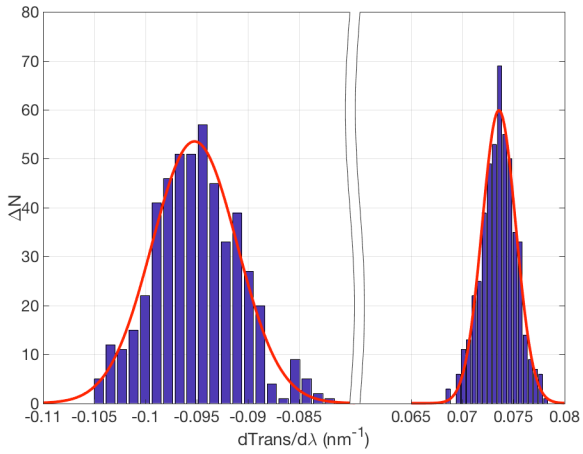

FIG. 7: The distribution of band-edge slopes constrained by the measured transmittance. Left histogram: $\frac{d\text{Trans}}{d\lambda}\big|_{\lambda_l,\Theta_l}$, with $\lambda_l = 915$ nm, $\Theta_l = (28.1 \pm 3.2)^\circ$. Right histogram: $\frac{d\text{Trans}}{d\lambda}\big|_{\lambda_r,\Theta_r}$ with $\lambda_r = 1064$ nm, $\Theta_r = (47.6 \pm 1.4)^\circ$.

(λ, θ) **value**	$\frac{d\text{Trans}}{d\lambda}$ K^{-1}	$\frac{d\text{Trans}}{dT}$ nm^{-1}	$f(\lambda,\theta)$ pm K^{-1}
LMA5** $\lambda_l = 915$ nm $\Theta_l = (28.1 \pm 3.2)^\circ$	-0.095 ± 0.004	$9.63 \pm 0.3 \times 10^{-4}$	-10.1 ± 0.5
LMA5** $\lambda_r = 1064$ nm $\Theta_r = (47.6 \pm 1.4)^\circ$	0.074 ± 0.002	$-6.87 \pm 0.3 \times 10^{-4}$	-9.3 ± 0.5
LMA5** $\lambda_0 = 1064$ nm $\Theta_0 = 0^\circ$	-	-	-8.7 ± 0.3

TABLE IV: Results for the motion of LMA5** at the band edges and at the center wavelength. Note that $\frac{d\lambda}{dT}$ is negative in all cases, indicating motion of the transmittance spectrum towards longer wavelengths with increasing temperature, or equivalently, movement of the wavelength axis towards the origin. The value for the motion of the center wavelength of the coating is calculated from the measurements of the motion of the two band-edges shown in the first two lines. If one assumes the silica values, α_L and β_L from Table I, $f(\lambda_0, \theta_0) = (-8.7 \pm 0.3)\,\text{pm K}^{-1}$, implies $\alpha_H + \beta_H/n_H = (12 \pm 0.4) \times 10^{-6}\,\text{K}^{-1}$

that gave the measured transmittance, we found that the band edge slope estimates varied much less.

Figure 5 illustrates the importance of constraining the theory to give the correct transmittance when estimating the band-edge slopes. Small variations in the angle of incidence, for example, would lead to large changes in the transmittance and correspondingly large variations in our estimate of the band-edge slope. However, if we fix the transmittance to the measured value, in other words, if we always sit at a known height on the band-edge, this sets the angle of incidence much more accurately than it can be measured directly and leads to a much better estimate of the band-edge slope. Similarly, if we allow the layer optical thicknesses to vary within their uncertainties but fix the height on the band-edge, only small angle of incidence changes (within the uncertainty) are required to accommodate the observed transmittance. The band-edge slope is then found to vary acceptably.

Figure 7 shows the distribution of band edge slopes from a Monte Carlo routine which took two inputs: the high and low index layer optical thicknesses, L_H and L_L. These were taken from Gaussian parent distributions with means at $\lambda_0/4$ and with standard deviation of 1% of the mean. (In other words, we assume 1% error in the layer thicknesses.) The angle of incidence was allowed to vary in order to obtain the measured transmittance at each band edge. The angle of incidence varies in this manner by an amount comparable to the uncertainty in our attempts to measure the angle directly. The range of band-edge slopes that emerges is thus reduced, indicating that the slope depends mostly on the transmittance itself and is much less sensitive to the coating layer thicknesses once the transmittance is set.

Table IV summarizes the results. The last row shows the center wavelength motion calculated from the band-edge motion measurements. We did this by applying the multilayer theory again, using another Monte-Carlo method. The coefficients of thermal expansion α_H, α_L and the thermo-optic coefficients β_H, β_L were drawn from gaussian distributions centered at the nominal val-

ues (from Table I and Section II A) with standard deviation equal to 50% of the nominal parameter values. (The choice of standard deviation is somewhat arbitrary. Allowing much larger standard deviations does not significantly affect the results.) For each iteration of the Monte-Carlo, i.e. for each random set of values $\alpha_H, \alpha_L, \beta_H, \beta_L$, we calculated the two band edge motions and the center wavelength motion. The center wavelength motion, plotted as a function of the two band edge motions is found to fall on a plane. By fitting a plane to the data, we expressed $f(\lambda_0, \Theta_0)$ as a linear combination of $f(\lambda_l, \Theta_l)$ and $f(\lambda_r, \Theta_r)$.

III. CONTRIBUTION TO β FROM TEMPERATURE-INDUCED COATING STRESS

Previous measurements of the thermorefractive properties of Ta_2O_5 have produced results for β that vary by about two orders of magnitude. The published values of β include 2.3×10^{-6} [30], 4.76×10^{-5} [31], and 1.21×10^{-4} [32]. Differences in deposition methods or annealing conditions may result in differing values for β but some of this variation may be due to temperature-induced coating stress.

Temperature induced coating stress and strain occur when the coefficients of thermal expansion of the substrate and coating materials don't match. The coating strain couples to the index of refraction through the stress-optical coefficient which leads to a strain-induced component of the thermo-optic coefficient. This is in addition to the material thermo-optic coefficient seen in an unconstrained coating. Therefore, the sample geometry and the substrate material can affect the measured thermo-optic coefficient, β. For example, in coated silicon cantilevers [33], this effect changed the measured thermo-optic coefficient by a factor of two.

The following estimate for the size of this effect in our own measurements assumes a semi-infinite substrate with a thin, single-layer coating. This results in no bending of the substrate so that coating expansion in the plane of the coating is identical to the substrate expansion. The temperature induced coating strain ϵ_c is given by the difference of the thermal expansion coefficients

$$\frac{\delta \epsilon_c}{\delta T} = \alpha_s - \alpha_c \tag{6}$$

where α_s and α_c are the substrate and coating thermal expansion coefficients, respectively. Isotropic materials under stress will exhibit a change in the index of refraction of that material [34, 35]

$$\beta_{strain} = \frac{\delta n}{\delta \sigma}\frac{\delta \sigma}{\delta T} = -\frac{1}{2} n^3 C_x E_c \frac{\delta \epsilon_c}{\delta T}. \tag{7}$$

Here C_x is the stress-optical coefficient of the coating and E_c is the Young's Modulus of the coating. The strain induced birefringence β_{strain} adds to the unstrained thermo-optic coefficient β_c of the coating to create an effective thermo-optic coefficient which is the one seen in measurements

$$\beta_{eff} = \beta_c + \beta_{strain} \tag{8}$$

A more general form of this result is given in equation 6.53 of [35] which also allows for coating anisotropy.

To estimate the magnitude of this effect, we consider a thin layer of Ta_2O_5 coated on a fused silica substrate. To the best of our knowledge, the stress-optic coefficient is not currently known for amorphous Ta_2O_5. However, many glasses are within an order of magnitude of SiO_2 [36]. If we assume the silica value, $C_x = 4.22 \times 10^{-12} \mathrm{m^2 N^{-1}}$ [34], we get $\beta_{strain} = 7.6 \times 10^{-6} \mathrm{K^{-1}}$. This is the same order of magnitude as reported values for β, so we should be cognizant of the effect when translating laboratory measurements to thermo-optic noise. In our measurements, the substrate material and the sample geometry are sufficiently similar to actual cavity mirrors that the measured β_{eff} is appropriate for estimating thermo-optic noise.

IV. COATING THERMO-OPTIC NOISE IN OPTICAL CAVITIES AND ADVANCED LIGO

Both the single layer and multilayer results allow us to calculate thermo-optic noise from the standard theory if we can rely on values of α_H measured elsewhere. Our multilayer results also allow us to go more directly to the thermo-optic noise as described below.

The optical phase accumulated by a laser beam upon reflection from a multilayer dielectric coating may be referred to a plane in front of the coating. See Fig. 8. Between this reference plane and the front surface of the coating, the beam accumulates a phase ψ_1 to approach the coating and ψ_2 departing, for a total free space phase accumulation $\psi = \psi_1 + \psi_2$. The phase accumulated by the beam during its actual interaction with the coating is $\theta = \mathrm{Arg}(\Gamma)$ where $\Gamma \in \mathbb{C}$ is the reflection coefficient of the mirror. The total reflected phase is then,

$$\phi = \psi + \theta. \tag{9}$$

As the mirror temperature rises, the phase θ accumulated within the coating changes because the layers expand and because the refractive indices of the layers also change with temperature. Our multilayer measurements lead directly to the value of $\frac{d\theta}{dT}$ for the coatings considered.

We relate the value $f(\lambda_0, \Theta_0)$ obtained from our measurements to the corresponding shift in the reflected phase, $\frac{d\theta}{dT}$. To do this, we found approximations (equations 11 & 12 below) describing the change with wavelength of the phase accumulated in the coating, $\frac{d\theta}{d\lambda}$. The chain rule then gives the accumulated phase change with temperature

$$\frac{d\theta}{dT} = \frac{d\theta}{d\lambda}\frac{d\lambda}{dT}. \tag{10}$$

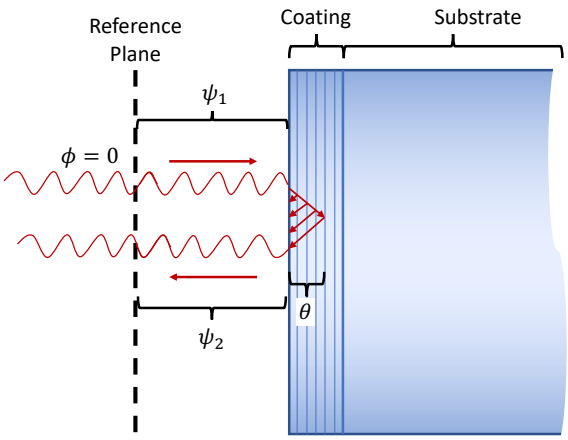

FIG. 8: Conventions for contributions to the reflected phase from a high reflective dielectric coating. The interaction of the beam with the coating is indicated schematically by the multiple reflections that together accumulate a total phase angle θ. The free space accumulation is $\psi = \psi_1 + \psi_2$. The total phase accumulation for a round trip between the reference plane and coating is $\phi = \theta + \phi$.

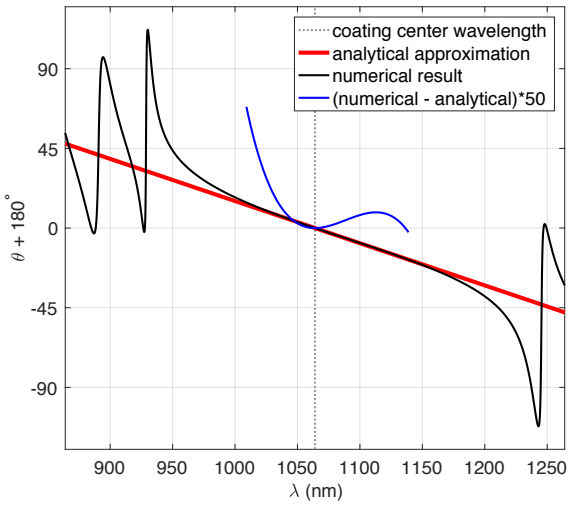

FIG. 9: The reflected phase for a 13 bilayer quarter wave stack near the center frequency λ_0. The analytical approximation to the slope $\frac{d\theta}{d\lambda}$ from Eq. (11)at the center frequency is shown in red. The residual, in blue, is magnified by a factor of 50 for wavelengths near the center frequency.

At the center wavelength λ_0 of a high-reflective quarter wave stack with $N \gtrsim 6$ layer pairs, $\frac{d\theta}{d\lambda}$ is approximately independent of the the number of layers. If the coating has no half-wave cap and the layer indices are arranged in the order

$$n_{\rm in} \left| n_H \right| n_L \left| n_H \right| n_L \left| \cdots\cdots \right|$$

where $n_{\rm in}$ is the index of refraction of the incident medium, and $n_H > n_L$, we find

$$\frac{d\theta}{d\lambda} = -\frac{\pi}{\lambda_0}\left(\frac{n_{\rm in}}{n_H - n_L}\right) \tag{11}$$

If the coating is covered by a half-wave cap of index $n_{\rm cap}$

$$n_{\rm in} \left| n_{\rm cap} \right| n_H \left| n_L \right| n_H \left| n_L \right| \cdots\cdots \left|\right.$$

the result is

$$\frac{d\theta}{d\lambda} = -\frac{\pi}{\lambda_0}\left(\frac{n_{\rm in}}{n_H - n_L} + \frac{2n_{\rm in}}{n_{\rm cap}}\right) \tag{12}$$

Figure 9 shows an example of the agreement between these analytical approximations and the full theory evaluated numerically. These analyticalal approximations for $\frac{d\theta}{d\lambda}$ are important because they show that while $\frac{d\theta}{d\lambda}$ is generally quite a complex function of wavelength and dependent on accurate knowledge of individual layer thicknesses, at the center wavelength of the coating, it becomes a simple function depending on only a few parameters. That allows us to estimate $\frac{d\theta}{d\lambda}$ with confidence despite the uncertainties in the coating layer thicknesses, etc. Figure 9 shows that use of this analytical approximations is well justified.

The power spectral density of temperature fluctuations in an optical coating appropriately weighted for interrogation by a TEM_{00} beam with Gaussian amplitude radius r_0 is [3, 7, 37]

$$S_T(\omega) = \frac{\sqrt{2}k_B T^2}{\pi r_0^2 \sqrt{\kappa\rho C}}\,\omega^{-\frac{1}{2}}\,. \tag{13}$$

The power spectral density of phase fluctuations induced on a beam reflected from a coating enduring these temperature fluctuations is then

$$S_\phi(\omega) = \left(\frac{d\phi}{dT}\right)^2 S_T(\omega) \tag{14}$$

$$= \left(\frac{d\theta}{dT} + \frac{d\psi}{dT}\right)^2 S_T(\omega). \tag{15}$$

$\frac{d\theta}{dT}$ is found from our measurements of $\frac{d\lambda}{dT}$ and applying Eq. (10). The free space phase accumulation ψ varies with temperature due to the thermal expansion of the coating as a whole

$$\frac{d\psi}{dT} = -\frac{4\pi}{\lambda}\bar{\alpha}_{\rm c} d \tag{16}$$

where λ is the optical wavelength, d is the coating thickness, and $\bar{\alpha}_c$ is the fractional thickness change of the optical coating per unit temperature. In the absence of direct measurements, $\bar{\alpha}_c$ is most accurately calculated by the method of [3] and [6] which takes into account the fact that the layers constrain one another from expanding freely in the plane of the layers. For simplicity, we use a weighted average of coating layer material values:

$\bar{\alpha}_c \approx \Sigma \alpha_i d_i/d$ where α_i are the thermal expansion coefficients of the individual coating layers and d_i are the layer thicknessess.

For an optical cavity consisting of two coated mirrors, the power spectral density of coating-induced thermo-optic noise in terms of cavity strain is then

$$S_h(\omega) = \left(\frac{\lambda}{2\pi L}\right)^2 \left[S_\phi^{\rm input}(\omega) + S_\phi^{\rm end}(\omega)\right] \qquad (17)$$

where L is the length of the cavity and the two terms refer to the input mirror and end mirror respectively. If we want to calculate the thermo-optic noise in a Michelson interferometer like Advanced LIGO, with two identical arm cavities, this result is multiplied by 2.

A. High Finesse Reference Cavities

Figure 10 shows coating thermo-optic noise in relation to other noise sources for a typical, 10 cm long, high finesse reference cavity with amorphous dielectric mirror coatings assumed to be similar to the titania-doped tantala coating measured in sections II B and II C. The coating thermo-optic noise was calculated using the method of Section IV together with the measurement of $\frac{d\lambda}{dT}$ from Section II C. The coating Brownian noise and substrate Brownian noise were found using [10, 15] with typical approximations (half-infinite substrate, coating treated as a homogeneous lossy layer). Coating Brownian noise dominates below 10 kHz. However, a factor of 10 reduction in coating Brownian noise beyond the level demonstrated by the best amorphous coatings has already been achieved in crystalline coatings. In such coatings, thermo-optic noise dominates the coating noise budget at frequencies above about 10 Hz [8]. Good estimates of thermo-optic noise in crystalline coatings will be needed to understand the noise budgets of the best high-finesse reference cavities.

B. Advanced LIGO and beyond

Thermo-optic noise is not a significant source of noise for the current generation of interferometric gravitational wave detectors but is likely to be a significant source of noise in future detectors. Figure 11 shows thermo-optic noise in relation to other noise sources in the current Advanced LIGO interferometers. Three curves are shown for thermo-optic noise corresponding to the three measurements presented in this paper for Ta_2O_5-based high index layers. We find that thermo-optic noise is a factor of about 4 below coating brownian noise at 100 Hz. The Gravitational Wave Interferometer Noise Calculator program, GWINC [38], was used to calculate the noise curves. The coating thermo-optic noise curves were calculated from the results of our measurements of

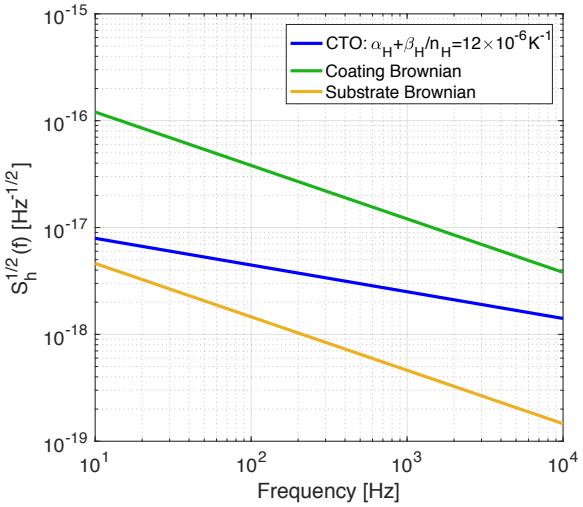

FIG. 10: Amplitude spectral density of coating thermo-optic noise (CTO), coating Brownian noise, and substrate Brownian noise in a typical high-finesse reference cavity. Cavity spacers supporting the cavity mirrors can also contribute significant Brownian noise, on the same order as the noise sources shown here [8]. (The level of thermal noise from spacers depends on spacer design details and we did not consider it here.)

$\alpha_H + \beta_H/n_H$, assuming $\alpha_H = 3.6 \times 10^{-6}$ from the literature (Table I) and $n_H = 2.17$ from our single layer measurements (Table II). GWINC implements the method in [3].

With better coating materials it is expected that coating Brownian noise in Advanced LIGO can be significantly reduced as has already been acheived in high-finesse reference cavities. Quantum noise in Advanced LIGO can also be further reduced [39]. At that point, thermo-optic noise will need to be considered in coating designs. As for future cryogenic interferometers, little is known about thermo-optic noise at low temperatures. Measurements of the relevant parameters at low temperatures will be needed to evaluate low temperature interferometer designs.

Acknowledgements

The authors would like to thank Gregory M. Harry for many helpful discussions and for coordinating the work within the broader Advanced LIGO coating research effort. Thanks also to Phil Willems who participated in some of the early brainstorming about how to measure the thermo-optic coefficient in amorphous thin films. Thanks to Harsh Menon who pointed us to the book and accompanying code by S.J. Orfanidis [40] that shed much light on the derivation of multilayer coating reflectivities. Thanks to Nour Ibrahim who assisted in making measurements of oven temperature uniformity. Thanks

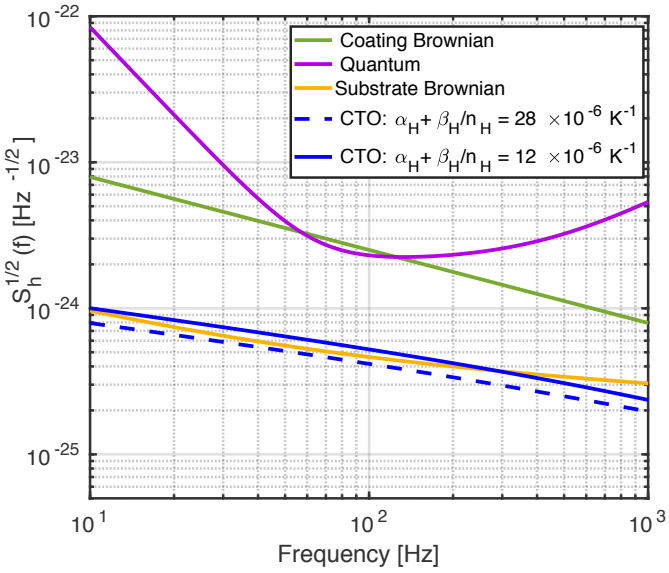

FIG. 11: Amplitude spectral density of selected contributions to the Advanced LIGO noise budget. The blue CTO curves correspond to measurements made in this paper. Solid line: Laser line measurement from Section II C. Dashed curve: Multilayer measurement from Section II B. The curve corresponding to the single layer result of Section II A is not shown since it is almost indistinguishable from the solid curve corresponding to the laser line result. The corresponding measured values are shown in the legend.

to Jason Jones of The University of Arizona for providing advice and guidance to one of the authors (EMG). Thanks to Darrel Smith who supported this research programmatically. This work was funded in part by the U.S. National Science Foundation under grants number NSF-0601135 and NSF-0757999.

[1] H. B. Callen and T. A. Welton, Phys. Rev. **83**, 34 (1951).
[2] H. B. Callen and R. F. Greene, Phys. Rev. D **86**, 703 (1952).
[3] M. Evans, S. Ballmer, M. Fejer, P. Fritchel, G. Harry, and G. Ogin, Physical Review D **78** (2008).
[4] V. B. Braginsky, M. L. Gorodetsky, and S. P. Vyatchanin, Phys. Lett. A **264**, 1 (1999), cond-mat/9912139, URL `https://www.sciencedirect.com/science/article/pii/S0375960199007859`.
[5] V. B. Braginsky and S. P. Vyatchanin, Physics Letters A **312**, 244 (2003), URL `http://arxiv.org/abs/cond-mat/0302617`.
[6] M. M. Fejer, S. Rowan, G. Cagnoli, D. R. M. Crooks, A. Gretarsson, G. M. Harry, J. Hough, S. D. Penn, P. H. Sneddon, and S. P. Vyatchanin, Phys. Rev. D **70**, 082003 (2004), gr-qc/0402034, URL `https://journals.aps.org/prd/abstract/10.1103/PhysRevD.70.082003`.
[7] V. B. Braginsky, M. L. Gorodetsky, and S. P. Vyatchanin, Phys. Lett. A **271**, 303 (2000), cond-mat/0008109, URL `https://arxiv.org/abs/cond-mat/0008109`.
[8] G. D. Cole, W. Zhang, M. J. Martin, J. Ye, and M. Aspelmeyer, Nature Photonics **7**, 644 (2013).
[9] P. Fritschel, Proceedings of SPIE Vol. 4856 "Gravitational Wave Detection", edited by Mike Cruise, Peter Saulson, (SPIE, Bellingham, WA, 2003) pp 282-291 (2003), URL `https://arxiv.org/abs/gr-qc/0308090`.
[10] G. M. Harry, H. Armandula, E. Black, D. R. M. Crooks, J. H. G. Cagnoli, P. Murray, S. Reid, S. Rowan, P. Sneddon, M. M. Fejer, et al., Applied Optics **45**, 1569 (2006), URL `https://www.osapublishing.org/ao/abstract.cfm?uri=AO-45-7-1569`.
[11] L. Barsotti, S. Gras, M. Evans, and P. Fritschel, Technical Note LIGO-T1800044-v5, Laser Interferometer Gravitational Wave Observatory (2018), URL `https://dcc.ligo.org/DocDB/0149/T1800044/005/T1800044-v5.pdf`.
[12] G. Harry, Tech. Rep. T040029-00-R, LIGO (2004).
[13] E. D. Black et al., Phys. Lett. A **328**, 1 (2004), gr-qc/0401034, URL `http://arxiv.org/abs/gr-qc/0401034`.
[14] G. M. Harry, A. M. Gretarsson, P. R. Saulson, S. E. Kittelberger, S. D. Penn, W. J. Startin, S. Rowan, M. M. Fejer, D. Crooks, G. Cagnoli, et al., Classical and Quantum Gravity **19**, 897 (2002).
[15] T. Hong, H. Yang, E. K. Gustafson, R. X. Adhikari, and Y. Chen, Phys. Rev. D **87**, 082001 (2013).
[16] M. Principe, Optics Express **23**, 10938 (2015).
[17] M. Abernathy, G. Harry, J. Newport, H. Fair, M. Kinley-Hanlon, S. Hickey, I. Jiffar, A. Gretarsson, S. Penn, R. Bassiri, et al., Physics Letters A **382**, 2282 (2018), in Press.
[18] A. Buonanno and Y. Chen, Phys. Rev. D **64**,

042006 (2001), URL http://prola.aps.org/abstract/PRD/v64/i4/e042006.

[19] S. Musikant, *Optical Materials* (Marcel Dekker Inc., 1985).

[20] R. W. Waynant and M. N. Ediger, *Electro-Optics Handbook* (McGraw-Hill Inc., 1994).

[21] G. V. Samsonov, *The Oxide Handbook* (IFI/Plenum, 1982).

[22] *Proceedings of the Symposium on Thin Films: Stresses and Mechanical Properties IV* (San Francisco, 1993).

[23] J. Mun, S. W. Kim, R. Kato, and e. a. I. Hatta, Thermochimica acta **455**, 55 (2007).

[24] D. R. M. Crooks, G. Cagnoli, M. M. Fejer, A. Gretarsson, G. Harry, J. Hough, N. Nakagawa, S. Penn, R. Route, S. Rowan, et al., Class. Quantum Grav. **21**, S1059 (2004).

[25] Z. Wu, M. Reichling, X. Hu, K. Balasubramanian, and et. al., Applied Optics **32**, 5660 (1993).

[26] G. M. Harry et al., Class. Quant. Grav. **24**, 405 (2007), gr-qc/0610004, URL http://arxiv.org/abs/gr-qc/0610004.

[27] Chuen-LinTien, C.-C. Jiang, C.-C. Lee, and K.-P. Chuang, J. of Mod. Opt. **47**, 1681 (2000).

[28] M. Abernathy, Ph.D. thesis, University of Glasgow (2012).

[29] M. Evans, in *GWADW 2008-VESF* (La Biodola, Isola d'Elba, Italy, 2008).

[30] A. Chu, H. Lin, and W. Cheng, Journal of Electrical Materials **26**, 889 (1997).

[31] S. Wiechmann and J. Müller, Thin Solid Films **517**, 6847 (2009).

[32] M. N. Inci, Journal of Physics D: Appl. Phys. **37**, 3151 (2004), URL http://iopscience.iop.org/article/10.1088/0022-3727/37/22/015/meta.

[33] W. Cheng, S. Chi, and A. K. Chu, Thin Solid Films **347**, 233 (1999).

[34] J. Stone, JOURNAL OF LIGHTWAVE TECHNOLOGY **6**, 1245 (1988), URL http://ieeexplore.ieee.org/stamp/stamp.jsp?tp=&arnumber=4122.

[35] G. Harry, T. P. Bodiya, and R. DeSalvo, *Optical Coatings and Thermal Noise in Precision Measurement* (Cambridge University Press, 2012).

[36] R. Waxler and A. Napolitano, Journal of Research of the National Bureau of Standards **59**, 121 (1957).

[37] Y. Levin, Physics Letters A **372**, 1941 (2008).

[38] URL https://git.ligo.org/gwinc.

[39] Y. Ma, H. Miao, B. H. Pang, M. Evans, C. Zhao, J. Harms, R. Schnabel, and Y. Chen, Nature Physics **13**, 776 (2017).

[40] S. J. Orfanidis, *Electromagnetic Waves and Antennas* (2016), URL http://www.ece.rutgers.edu/~orfanidi/ewa/.

[41] For the Ta_2O_5 coating, the slope of the trend is about $\frac{\mathrm{d}}{\mathrm{d}\lambda}\left(\frac{1}{L}\frac{dL}{dT}\right)$ = -1.5 $\times$ 10^{-8} $\mathrm{nm}^{-1}\mathrm{K}^{-1}$ intersecting λ = 500 nm at 1.34×10^{-5} K^{-1}. Extrapolating the trend gives $\alpha + \beta/n = 5 \times 10^{-6}$ at $\lambda = 1064$ nm.